Hydroclimate change in subtropical South Africa during the mid-Piacenzian Warm Period

Xueqin Zhao, Andreas Koutsodendris, Thibaut Caley, Lydie Dupont

Hydroclimate change in subtropical South Africa during the Mid-Piacenzian Warm Period

Xueqin Zhao[1], Andreas Koutsodendris[2], Thibaut Caley[3], Lydie Dupont[1]

[1] MARUM - Center for Marine Environmental Sciences, University of Bremen, Leobener Straße, D-28359 Bremen, Germany

[2] Institute of Earth Sciences, Heidelberg University, Im Neuenheimer Feld 234-236, D-69120 Heidelberg, Germany

[3] EPOC, UMR 5805, CNRS, University of Bordeaux, Pessac, France

Abstract

The mid-Piacenzian Warm Period (mPWP, 3.264-3.025 Ma) of the Pliocene epoch has been proposed as an analog for future climate scenarios. Disagreement between the paleoenvironmental reconstruction and model simulations of the climate in subtropical regions for this period suggests that more investigation of the subtropical climate variability of the mPWP is needed. This study presents pollen, microcharcoal and benthic foraminifera oxygen isotope records generated from marine sediment cores of International Ocean Discovery Program (IODP) Exp. 361 Site U1479 from the Cape Basin offshore of South Africa for the period between 3.337 and 2.875 Ma. With an average sample resolution of 3 ka, this record represents the highest-resolution record of mPWP vegetation change from the region. Our results indicate that the vegetation during the mPWP was dominated by fynbos (species-rich heathy vegetation in the Cape Floristic Region) with variable proportions of Ericaceae. Moreover, the development of the Afrotemperate forest (tall, multilayered indigenous forests in South

Africa) reflects shifts in the amounts of precipitation between winter and summer in the year-round rainfall zone. The vegetation variation is probably influenced by the latitudinal insolation gradient in response to precession forcing. Several glacials depicted by the benthic foraminifera oxygen isotope record were characterized by lower percentage values of Restionaceae, higher percentage values of ericoid fynbos and Afrotemperate forest. These events correspond well with cooler SE Atlantic sea surface temperatures driven by interactions of both atmospheric and oceanographic processes. The cooler sea surface temperatures attributed to Antarctic ice sheet expansion, reduced Agulhas leakage (heat and salt transfer from the Indian Ocean to the Atlantic Ocean) and/or intensified southern Benguela upwelling, resulted in less precipitation in the winter rainfall zone of South Africa.

Keywords: Vegetation, hydroclimate, mid-Piacenzian Warm Period, IODP Site U1479, South Africa

1. Introduction

The mid-Piacenzian (mid-Pliocene) Warm Period (mPWP, 3.264–3.025 Ma) of the Pliocene epoch was the most recent period in geological history in which global climate was warmer than today as depicted by both paleoclimate data and modelling studies (Haywood et al., 2013). During that period, paleogeography, paleoceanography and paleobiology were the same or very similar to the modern situation (Crowley, 1996) making the mPWP a suitable analog for future climate scenarios (Haywood et al., 2009, 2013). On this basis, the mPWP has become the focus of comparative and detailed numerical climate modelling and data/model comparisons. The simulated global temperatures during the mPWP were approximately 2–3°C higher than today (Haywood and Valdes, 2004) and atmospheric CO_2 concentrations (between 330 and 400 parts per million) were estimated to be 50-120 ppm higher than pre-industrial levels (275-285 ppm) and probably close to today's level (Pagani et al., 2010). Average global sea level was 10–40 m higher than today (Raymo et al., 2011), the extent of continental ice sheets was limited (Dolan et al., 2011), and the Atlantic meridional overturning circulation (AMOC) was comparable to or stronger than during pre-industrial times (Raymo et al., 1996).

However, it remains unclear what mechanisms drove the amplification of warm conditions during the mPWP. Previous studies including paleoclimate modelling, micropaleontological paleotemperature records and paleo-CO_2 estimates based on the boron isotopes of planktic foraminifers, have focused on the role of the atmosphere and oceans, in particular that of ocean-atmospheric CO_2 levels and changes in the meridional ocean heat flux (Bartoli et al., 2011; Dowsett et al., 1992; Rind and Chandler, 1991). Later studies, however, suggest additional drivers of the warmer Pliocene conditions independently or in combination with CO_2 concentration variations

(Haywood et al., 2009). Salzmann et al. (2008) proposed that the potential causes for the mPWP have only been partially identified. These causes may relate to a combination of changes in orography, atmospheric CO_2 concentrations, water vapor content, ocean circulations and ocean heat transport (Crowley, 1996; Lunt et al., 2012; Raymo et al., 1996), which in turn affect changes in sea-ice cover, surface albedo, cloud cover and temperature (Haywood and Valdes, 2004).

Although the climate of the middle Pliocene is relatively stable compared to the Quaternary, it does display climate variability on orbital timescales (Lisiecki and Raymo, 2005), which can be interpreted to represent glacial-interglacial periods (Lunt et al., 2012). Just prior to the mPWP, the middle Pliocene was interrupted by a short intense global glaciation (3.305–3.285 Ma) during marine isotope stage M2 (MIS M2) (Lisiecki and Raymo, 2005), which may be seen as a premature step of the climate system in establishing an ice age world (De Schepper et al., 2009; Prell, 1984). The mPWP encompasses six interglacials and glacials including the glacial MIS KM2. Earlier studies compared separately modelled interglacials within the mPWP. The results show that different orbital boundary conditions lead to considerable differences in simulated climate and vegetation between the warm stages (Prescott et al., 2018).

We collected summarized paleovegetation studies of the middle and late Pliocene based on pollen or carbon isotopic composition of pedogenic carbonate and mammal teeth. The results show consistency with modern vegetation (Figure 1), however, due to the lack of records in the southern hemisphere, it should be interpreted with caution. Many paleoclimate studies indicate that the vast northern and southern subtropical regions were wetter during the Miocene and Pliocene with a spread of tropical savannahs and woodland where subtropical deserts and arid regions exist today (Salzmann et al., 2008), in particular in Africa (Levin, 2015) and Australia (Martin, 2006).

However, most models predict drier conditions during past warm climates including the warm Pliocene (Lau et al., 2013). This puzzle is explained by weaker atmospheric circulation in response to reduced meridional and zonal temperature gradients (Burls and Fedorov, 2017).

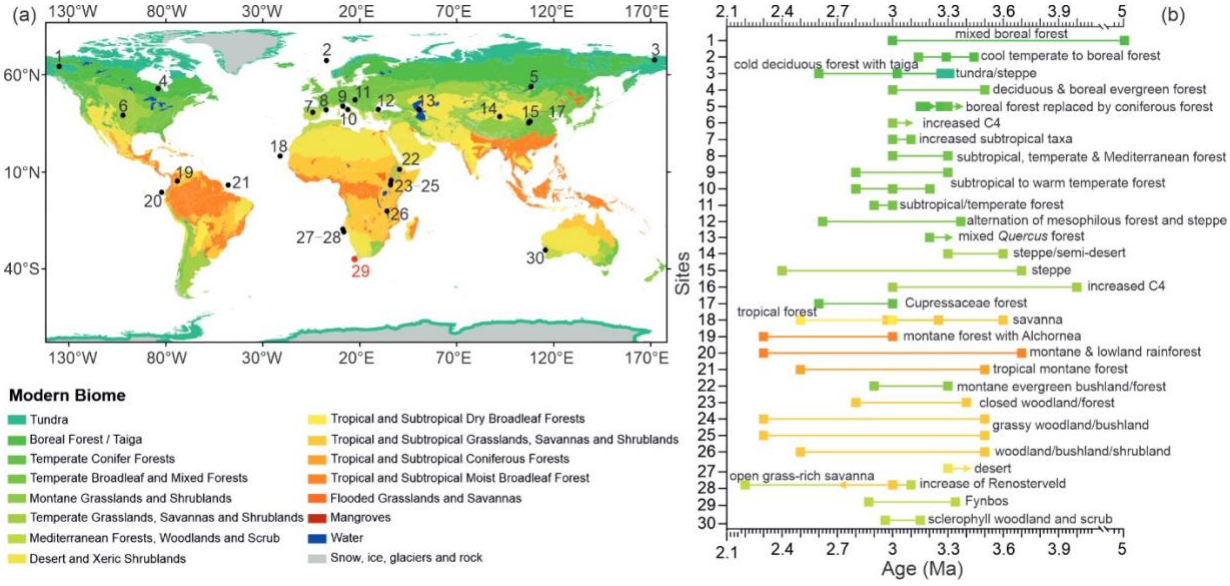

Figure 1. Modern biomes (a) and paleovegetation records between 5 and 2.2 Ma (b). The colors in (b) correspond to the modern terrestrial biomes which are derived from the World Wildlife Fund (WWF) ecoregions depicted in (a). The Y-axis “Sites” in (b) corresponds to the numbers in (a). Detailed data sources of (b) can be found in Supplementary file 1.

Southern Africa has experienced strong regional differences in moisture availability (Chase and Meadows, 2007; Zhao et al., 2016b) due to the interactions of both atmospheric and oceanic circulations between the South Atlantic, Indian and Southern Oceans. The combination of palynological, geomorphological and sedimentological evidence indicates warm mesic conditions in southern Africa during the mid-Pliocene (Scott and Partridge, 1994). A mixture of shrubland (fynbos), woodland and forest prevailing in South Africa during the mid-Pliocene suggests more humid conditions (Salzmann et al., 2008). On the other hand, the model study by Prescott et al. (2018) infers dominance of shrubland and desert instead of forest and woodland in South Africa during all four mPWP interglacials (G17, K1, KM3 and KM5c). Moreover, other

models also predict less annual rainfall and less winter rainfall for Pliocene South Africa (Hunter et al., 2019). First data-model comparisons (the Pliocene Model Intercomparison Project Phase 2; PlioMIP2), mainly concerning sea surface temperatures, have been carried out (Haywood et al., 2020, accepted). The results show significant agreement between simulated and reconstructed temperature change although with notable local signals of data/model disagreement occurring in the Benguela upwelling system. The large data/model discrepancy in the Benguela upwelling system is also observed in SST anomalies focusing on MIS KM5c (3.205 Ma) (the warmest phase of the mPWP), which might be accounted for by a combination of displaced upwelling and warm upwelled water (McClymont et al., 2020). These data-model mismatches indicate that more detailed mPWP hydroclimate reconstructions of subtropical regions are needed, especially in the southern hemisphere where well-dated high-resolution Pliocene paleorecords are scarce. As such, a new record from the South African Cape region at the intersection of the different atmospheric and oceanic systems between the South Atlantic, Indian and Southern Oceans is essential to fill in a gap of information on the southern hemisphere subtropical regions. Thus, to better understand the hydroclimate of subtropical southern Africa during the mPWP, we produced a continuous high-resolution pollen, microcharcoal and benthic foraminifera oxygen isotope record from marine sediment cores of IODP Exp. 361 Site U1479 for the period between 3.337 and 2.875 Ma at millennial-scale resolution (ca. 3 ka) (Figure 2). The aim of our study is to assess the variability of vegetation and climate changes in southernmost Africa during the mPWP and to determine possible driving mechanisms.

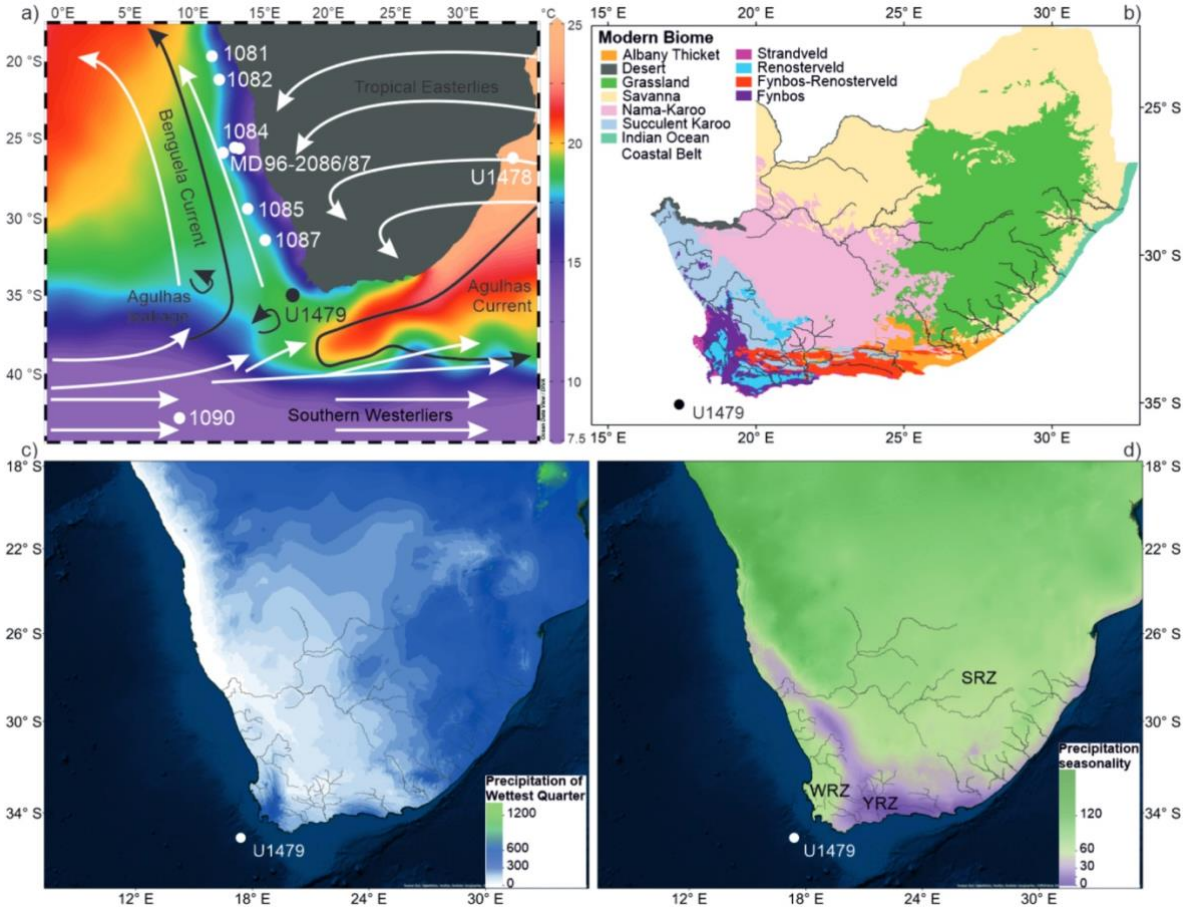

Figure 2. (a) Map of modern atmospheric and oceanic circulations with modern sea surface temperatures (World Ocean Atlas 2013) and the location of IODP Site U1479 and the other sites discussed in this study. (b) Modern vegetation of South Africa with main rivers draining to the ocean (Mucina and Rutherford, 2006). Modern precipitation of wettest quarter (c) and precipitation seasonality (d) showing three different rainfall zones in southern Africa derived from WorldClim version 1.3 (Hijmans et al., 2005). Winter rainfall zone, WRZ, at the southwestern tip of the continent which receives over 66% of annual rainfall between April and September; year-round rainfall zone, YRZ, which receives both winter and summer rainfall throughout the year (purple); summer rainfall zone, SRZ, in the rest of the subcontinent which receives over 66% of annual rainfall between October and March.

2. Regional setting

2.1 Climate and oceanic circulation

Modern climate of southern Africa is controlled by the position and strength of the South Atlantic and the Indian Ocean anticyclones (Shannon and Nelson, 1996) (Figure

2), which results in three different rainfall zones from west to east of South Africa: winter rainfall zone (WRZ), year-round rainfall zone (YRZ) and summer rainfall zone (SRZ) (Tyson and Preston-Whyte, 2000). The pressure difference between the South Atlantic anticyclone and the continental pressure field causes alongshore southeast trade winds (SE trade winds). The SE trade winds drive an offshore, surface-drift inducing Benguela upwelling causing aridity in western southern Africa north of the Cape region. In the Cape region, moisture is mainly supplied by the southern westerlies during austral winter. The northern part of the WRZ is relatively arid due to the all-year influence of the cold waters of the Benguela upwelling system. The influence of westward to south-westward directed offshore winds (known as Berg winds) is very limited because they are blocked by the southern westerlies and almost no dust plumes can be observed south of 28°S (Eckardt and Kuring, 2005). The SRZ receives most of its rainfall from tropical moisture easterlies during austral summer. In contrast to the pronounced seasonality in the WRZ and SRZ, an intermediary area between them is the YRZ influenced by the interaction of both temperate and tropical circulation systems. In the YRZ, at least 11 but mostly all 12 months of the year contribute 5% or more to the long-term average of the total annual rainfall during 1979–2011 (Engelbrecht et al., 2015).

Rainfall amounts, seasonality and distribution patterns in southern Africa are further influenced by two major oceanic circulation systems (Figure 2). One is the northward flowing Benguela Current (BC) along the west coast of southern Africa, the other is the Agulhas Current (AgC) (Nelson and Hutchings, 1983; Shannon and Nelson, 1996). At the southern boundary of the Benguela upwelling system, the relatively cool and oligotrophic waters of the South Atlantic Current and the cold waters of the Antarctic Circumpolar Current meet the south-westward flowing warm and saline waters of the Agulhas Current. Most of the AgC waters are retroflected to the south and east forming

the Agulhas Return Current, while a small part of the AgC continues in a north-westerly direction through the South Atlantic Ocean in the form of eddies. The leakage is determined mainly by the latitudinal position and intensities of the southern westerlies. During austral summer, the southward contraction and intensification of the southern westerlies would favor more Agulhas leakage, coinciding with aridity in the WRZ (Biastoch et al., 2009; Durgadoo et al., 2013).

IODP Exp. 361 Site U1479 is located on the western slope of the Agulhas Bank in Cape Town under the pathway of mixed water masses: southward flowing North Atlantic deep water, cold northward-flowing Benguela Current, warm and salty Agulhas leakage (Hall et al., 2017).

2.2 Vegetation and fire

The strong west-east gradient in rainfall amount and seasonality has a great effect on the vegetation resulting in nine biomes in southern Africa (Figure 2) (Cowling et al., 1997; Mucina and Rutherford, 2006). The continental area near the study site is dominated by vegetation types including Fynbos, Renosterveld, Succulent Karoo and Nama Karoo. In addition, small patches of Afrotemperate Forest occur.

Subtropical regions are equatorward defined by the transition from subtropical to tropical (monsoonal) climates. The rainfall season changes from summer rains in the tropics to winter rains in the subtropics, which has a large impact on vegetation. In southern Africa, the subtropical winter rainfall zone (Chase and Meadows, 2007) is nowadays restricted to the Western and Southern Cape Province, which is mainly dominated by fynbos (Linder, 2003). **Fynbos** is a species-rich heathy vegetation, which was established in South Africa during the late Miocene (Dupont et al., 2011). The Fynbos biome, part of the Cape Floristic Region, has extremely high levels of species richness and endemism. It is an evergreen, fire-prone shrubland in the

194 southwest Cape, which is typified by the presence of restios (wiry, evergreen
195 graminoids of the Restionaceae), a high cover of ericoid shrubs (fine-leaved shrubs of
196 Ericaceae, Asteraceae, Rhamnaceae, Thymelaeaceae and Rutaceae), and the
197 common occurrence of proteoid shrubs (Proteaceae). Rainfall usually varies from 600
198 to 800 mm/yr. Other important features of fynbos are the presence of leaf spinescence,
199 high sedge (Cyperaceae) cover and low grass (Poaceae) cover (Mucina and
200 Rutherford, 2006). Fynbos is found especially along the southwestern and southern
201 coast of South Africa and thus receives most rainfall during austral winter.
202 **Renosterveld** is an evergreen, fire-prone shrubland or grassland, which is dominated
203 by small, cupressoid-leaved and evergreen asteraceous shrubs (principally
204 renosterbos, *Elytropappus rhinocerotis*). Other important shrub represented in
205 renosterveld include Boraginaceae, Fabaceae, Malvaceae, *Cliffortia* and
206 *Anthospermum* (Goldblatt and Manning, 2002). The **Succulent Karoo** biome, located
207 in a narrow strip inland of the west coast, is a semidesert region characterized by dwarf
208 leaf-succulents of which Aizoaceae (including Mesembryanthemoideae) and
209 Crassulaceae are particularly prominent; many other families are also common
210 including Asteraceae, Amaranthaceae, Euphorbiaceae (*Euphorbia*) and
211 Zygophyllaceae (*Zygophyllum*) (Wheeler, 2010) but grass cover is low. In comparison
212 to the Fynbos biome, the Succulent Karoo biome is better adapted to arid conditions
213 and higher summer temperatures (Carr et al., 2014), receiving most of the rainfall
214 during austral winter. The **Nama Karoo** biome, which is a semi-desert dwarf and
215 grassy shrubland found on the central plateau, is dominated by Asteraceae, Poaceae,
216 Aizoaceae, Liliaceae and Scrophulariaceae. The Nama Karoo biome located northeast
217 of the study area, receives rainfall mainly during austral summer. The **Afrotemperate**
218 **Forest** biome, which is restricted to areas with mean annual rainfall of more than 725
219 mm in the SRZ and more than 525 mm in the WRZ (Mucina and Rutherford, 2006)

comprises mostly of evergreen trees in multi-layered canopies, while the ground layer is often poorly developed due to the dense shade. The southern Afrotemperate forest occurs in patches near Port Elizabeth in the east to Cape Peninsula in the west along the feet of south and east-facing slopes, and in ravines and deep gorges of the Cape Fold Belt mountains (Bergh et al., 2014). These forests reach their greatest extent in the southern Cape along the narrow (ca. 250 km long) coastal strip between Humansdorp in the east to the west of Mossel Bay (Bergh et al., 2014).

Fire is important in the fynbos ecosystem, which burns on a 5–50 year rotation, usually in the order of 15–25 years (Mucina and Rutherford, 2006). Fire regimes in Renosterveld are largely unknown; it is however assumed that fire rotation lies within a 2–10 year range. Presently, fires occur in late summer and early autumn, towards the end of the dry season naturally due to sparks of rockfalls and lightning (Bond, 1996; Van As et al., 2012).

The YRZ also plays an important role in fostering the extraordinary botanical diversity of the region (Mucina and Rutherford, 2006; Bergh et al., 2014). In the southern Cape region, there is a mosaic of various vegetation types of fynbos as well as Afrotemperate forest and coastal thicket. Generally, Afrotemperate forest patches require the highest values of soil moisture (average annual rainfall varies between 500 and 1200 mm) (Mucina and Rutherford, 2006) and are thus most prominent in the valleys, whereas fynbos and coastal thicket occur in the coastal lowlands and dunes (Quick et al., 2018). Afrotemperate forest in this region can be found within the Touws River and Duiwe River valleys which are dominated by *Afrocarpus falcatus*, *Podocarpus latifolius* and *Olea capensis* (Cowling et al., 1997).

3. Materials and methods

3.1 Materials and age model

The samples investigated in this study were collected from sediment cores of IODP Exp. 361 Site U1479 (35°03.52'S, 17°24.03'E, ~2630 m water depth). Site U1479 is located in the Cape Basin on a 30 km wide morphological high, rising ~200 m above the regional seafloor on the mid to lower western slope of the Agulhas Bank, ~130 km southwest of Table Mountain and Cape Town, South Africa (Hall et al., 2017). Material from the undisturbed Holes U1479B and U1479C were selected to obtain a complete spliced stratigraphic section from the best core parts using color and natural gamma ray data. The photos of the cores can be found on the IODP website with the following link (http://publications.iodp.org/proceedings/361/EXP_REPT/CORES/IMAGES/). The original meter composite depth was updated to an adjusted, so-called composite depth below seafloor (m CCSF-A). The study interval was first defined based on the shipboard age model, which was developed using bio- and magnetostratigraphy (Hall et al., 2017). The final age model across the study interval was further refined by tuning of benthic foraminifera oxygen isotope curves to the global LR04 benthic $\delta^{18}O$ stack (Lisiecki and Raymo, 2005) using the AnalySeries software (Paillard et al., 1996) and yielded a correlation coefficient of R = 0.81 for the studied time interval. It provides a continuous record between 3.337 and 2.875 Ma. The sedimentation rates of the investigated interval between 141.24 and 164.07 m CCSF-A lie between 4.1 and 6.8 cm/ka (an average of 5.0 cm/ka).

3.2 Benthic foraminifera $\delta^{18}O$ analysis

Specimens of benthic *Cibicides wuellerstorfi* foraminifera were picked from the 250–315 µm size fraction.

76 samples were measured with a MultiPrep system on line with a dual Inlet IsoPrime™ Isotope Ratio Mass Spectrometer (IRMS) at the Laboratoire de Geologie of the University of Lyon. Calcium carbonates were reacted with anhydrous phosphoric

acid at 90°C to generate CO_2. Isotope compositions are quoted in the delta notation in ‰ relative to Vienna Pee Dee Belemnite (VPDB). Isotopic data result from a one-point calibration using the internal reference 'Carrara Marble' (Analytical standard deviation of 0.05‰ for $\delta^{18}O$ with a carbonate weight >100µg and 0.1‰ with a carbonate weight <100µg), itself regularly calibrated against the international reference NBS19.

17 samples were carried out on a Thermo Scientific 253 Plus isotope ratio mass spectrometer coupled to a Kiel IV carbonate device at EPOC laboratory, University of Bordeaux. The automated preparation system (Kiel IV) transforms solid carbonate samples into CO_2 gas by treatment with orthophosphoric acid at a constant temperature of 70°C. The sample CO_2 gas is then transferred using a microvolume, and introduced by dual inlet in the Mass spectrometer to measure its $^{18}O/^{16}O$ isotopic ratio in comparison with a calibrated reference gas. Aliquots of NBS19 standard, which is calibrated against the VPDB, were analyzed with the samples to correct any deviation of the reference gas. Oxygen isotopic ratio values are expressed using the δ notation with a per mil deviation (‰) from VPDB. Analytical standard deviation is ≈ 0.06‰ for $\delta^{18}O$.

In three of the samples analyzed in this study no *Cibicides wuellerstorfi* could be found. We, therefore, analyzed $\delta^{18}O$ on *Uvigerina peregrina* taxa in the same size fraction. Because *Uvigerina peregrina* is isotopically heavier than *Cibicides* by 0.47‰, we adjusted *Uvigerina peregrina* $\delta^{18}O$ to the *Cibicides* scale by subtracting 0.47‰ according to Marchitto et al. (2014). Benthic foraminifera $\delta^{18}O$ are available and stored in the Pangaea database (https://doi.pangaea.de/10.1594/PANGAEA.919576).

3.3 Palynological analysis

A total of 151 samples were taken at 15 cm intervals between 141.24 and 164.07 m CCSF-A for palynological analysis, aiming at a temporal resolution of ca. 3 ka. The samples were prepared with the following steps: 1) determination of the sample volume by water replacement; 2) decalcification with diluted cold HCl (~10%) and addition of *Lycopodium* spore tablets (12 samples with 2 tablets of batch Nr. 4832162 and the other 139 samples with 2 tablets of batch Nr. 177745); 3) after washing, the samples were treated with cold HF (~40%); 4) the samples were shaken for 2 hours, and then kept standing for two days to remove silicates; 5) concentrated HCl (~37%) was added to keep fluor-complexes in solution; 6) all samples were first sieved over a 125 µm metal mesh and then sieved over a 7-µm nylon mesh screen while ultrasonically disaggregating organic matter; 7) samples were stored in water, mounted in glycerol and examined under a light microscope (magnification 400 x and 1000 x) for pollen, spores, fresh-water algae, and microcharcoal. Pollen grains were identified using the African pollen reference collection of the Department of Palynology and Climate Dynamics of the University of Göttingen, the African Pollen Database (http://apd.sedoo.fr/pollen/interface/indexPollen.html) and literature (Bonnefille and Riollet, 1980; Scott, 1982). Pollen zonation was conducted by Constrained Incremental Sum of Squares Cluster Analysis (CONISS, TILIA 2.0.41, with dendrogram scale of total sum of squares) including all counted pollen and spore taxa (Figure 3). All pollen and spore taxa were included in the pollen sum (ranging between 145 and 347 with an average of 290 per sample) used to calculate pollen percentages. Pollen concentration was determined based on the *Lycopodium* spore counts. Samples volumes were measured using water displacement to calculate concentration values. Pollen accumulation rates were calculated by multiplying the pollen concentration (grains/cm^3) by the sedimentation rate (cm/ka) for each sample. The 95% confidence intervals of percentages were calculated following Maher (1972). All counts of pollen and spores

are available and stored in the Pangaea database (https://doi.pangaea.de/10.1594/PANGAEA.919633). Microcharcoal analysis was conducted on the same slides as the pollen analysis using the 202-touch point count method (Clark, 1982) to calculate the microcharcoal concentration in square centimeter/cubic centimeter (cm^2/cm^3). At least 225 fields per sample were analyzed to improve the statistical reliability of the results. Microcharcoal concentrations are available and stored in the Pangaea database (https://doi.pangaea.de/10.1594/PANGAEA.919575).

3.4 Spectral analysis

To analyze cyclicity in the palynological records, we carried out a spectral analysis (window: hanning; oversample: 2; segments: 3) using the module REDFIT (Schulz and Mudelsee, 2002) of the paleontological statistics package PAST vs 3.0 (Hammer et al., 2001).

A cross spectral analysis between pollen groups and southern hemisphere latitudinal winter insolation gradient (LIG) was also carried out with AnalySeries software (Paillard et al., 1996). Linear interpolation was used to resample data and LIG according to the pollen resolution. For each analysis, B-Tukey spectrum was used within a Bartlett window. The time step used for the B-Tukey analysis is 2000 years. The bandwidth is 1.07×10^{-5}, non-zero coherence significant at the 95% confidence level is higher than 0.55.

4. Results

Pollen and spores are relatively abundant and generally well preserved in IODP Site U1479 for the period 3.337 to 2.875 Ma. Pollen concentrations range from 289 to 1037 grains/cm^3 with an average of 533 grains/cm^3 and pollen accumulation rates range

from 1.2×10^3 to 5×10^3 grains/cm^2/ka with an average of 2.7×10^3 grains/cm^2/ka. The pollen diagram of selected pollen taxa for the period from 3.337 to 2.875 Ma is provided in Figure 3. The most abundant pollen taxa throughout the record are Restionaceae (~18–44%, average 33%), Cyperaceae (~9–26%, average 18%), Tubuliflorae (~4–15%, average 9%), Podocarpaceae (~1–15%, average 5%), Poaceae (~2–11%, average 6%). Other common pollen taxa include *Stoebe-Elytropappus*-type (~0–7%, average 2%), Ericaceae (~1–8%, average 4%), CCA (including Amaranthaceae, and Caryophyllaceae) (~0–9%, average 3%), *Cliffortia*-type (~0–3%, average 0.7%), *Passerina* (~0–3%, average 0.6%), *Protea*-type (~0–4%, average 1%), *Phragmitis*-type (~0–7%, average 2%), *Artemisia*-type (~0–3%, average 0.7%), *Anthospermum* (~0–4%, average 0.8%), *Pentzia*-type (~0–4%, average 2%) and *Euphorbia* (~0–3%, average 0.6%).

The identified pollen was grouped into vegetation categories (Figure 4) as ericoid fynbos (including *Stoebe-Elytropappus*-type, Ericaceae, *Cliffortia*, *Passerina*, other Thymelaeaceae, *Protea*-type), wetland taxa (including Cyperaceae, *Phragmites*-type, *Typha*, Haloragaceae), cosmopolitan taxa (including Poaceae, Asteraceae Tubuliflorae, *Artemisia*-type, *Anthospermum*, Euphorbiaceae pp), succulent and drought-resistant taxa (including *Pentzia*-type, Amaranthaceae, Aizoaceae, *Euphorbia*) and Afrotemperate forest (including Podocarpaceae, *Olea*-type). This grouping is based on the modern pollen distribution in the Namaqualand mudbelt along the west coast of South Africa (Zhao et al., 2016a, 2016b) and on palynological studies from the Cederberg Mountains (Valsecchi et al., 2013) and the south coast (Quick et al., 2018).

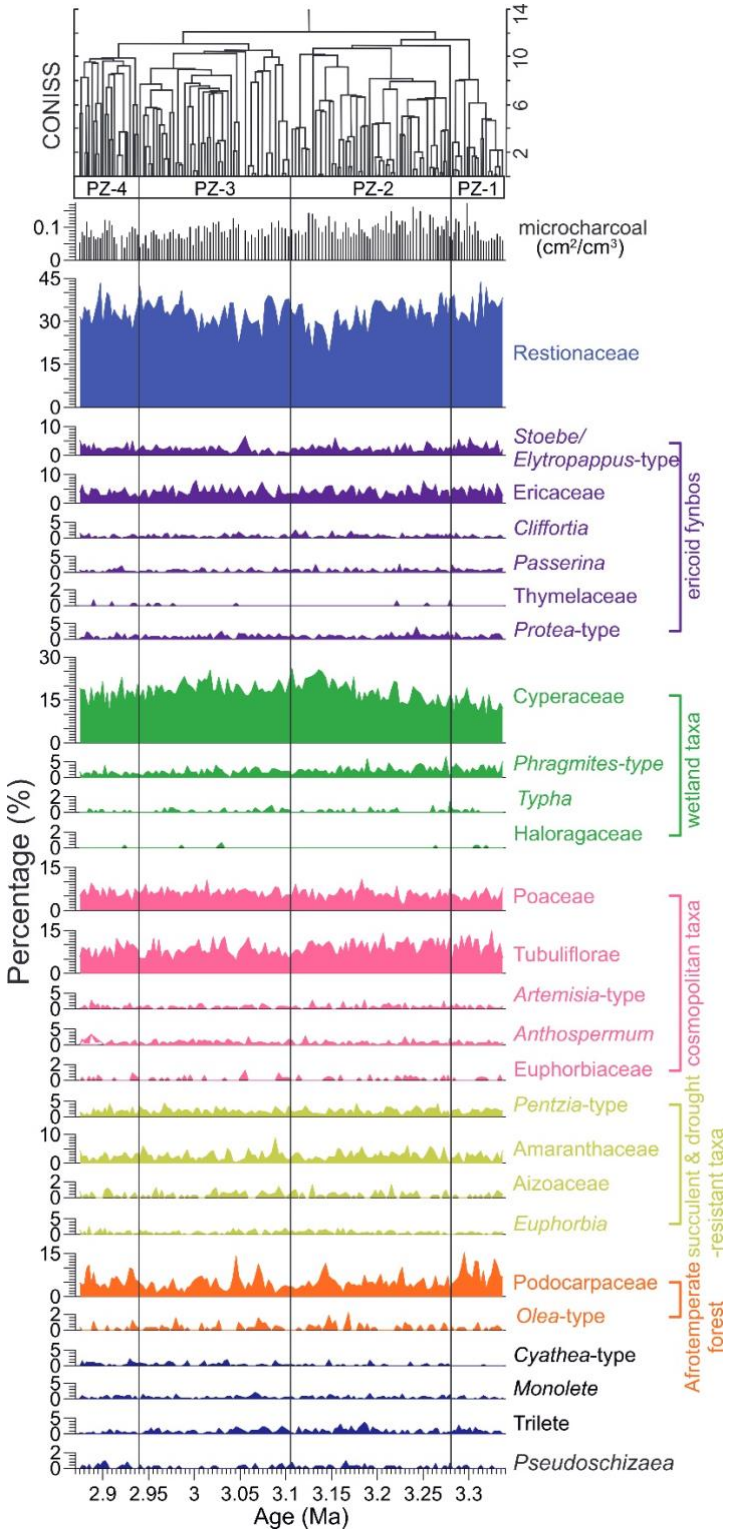

366

367 **Figure 3**. Pollen percentages of selected taxa from IODP Site U1479. Pollen assemblage zones were
368 derived by CONISS (Grimm, 2015).

369 The record has been divided into four pollen assemblage zones (PZ) using the
370 CONISS calculation (Grimm, 2015). Zone PZ-1 (3.337–3.280 Ma) is characterized by
371 pollen percentage maxima of Restionaceae, ericoid fynbos and Afrotemperate forest.

The percentages of succulent and drought taxa, and Cyperaceae reach minima in this zone. Zone PZ-2 (3.280–3.107 Ma) is characterized by a pollen percentage decrease of Restionaceae reaching minima around 3.147 Ma, while ericoid fynbos reaches high values around the same time. Afrotemperate forest representation has much lower values in PZ-2 than in PZ-1 but shows several peaks. Succulent and drought taxa start to increase to high values between 3.279 and 3.156 Ma. This zone is also characterized by the increase of wetland taxa reaching maxima around 3.136 Ma. In zone PZ-3 (3.107–2.941 Ma), the pollen percentage of Restionaceae starts to increase again, while the percentage of wetland taxa fluctuates around relatively high values with slightly decreasing trend. Succulent and drought taxa fluctuate with no clear trend. Zone PZ-4 (2.941–2.875 Ma) shows alternating percentage maxima of Restionaceae and Afrotemperate forest.

Microcharcoal concentration values fluctuate between 0.04 and 0.17 cm^2/cm^3 with an average of 0.09 cm^2/cm^3 (Figure 4). Microcharcoal concentrations are characterized by relatively low values at the beginning of the record with a generally increasing trend until 3.239 Ma and a maximum of 0.17 cm^2/cm^3 at 3.298 Ma. After 3.239 Ma, microcharcoal concentrations start to decline reaching minimum values (0.04 cm^2/cm^3) at 2.950 Ma which then increase to higher values again after 2.941 Ma.

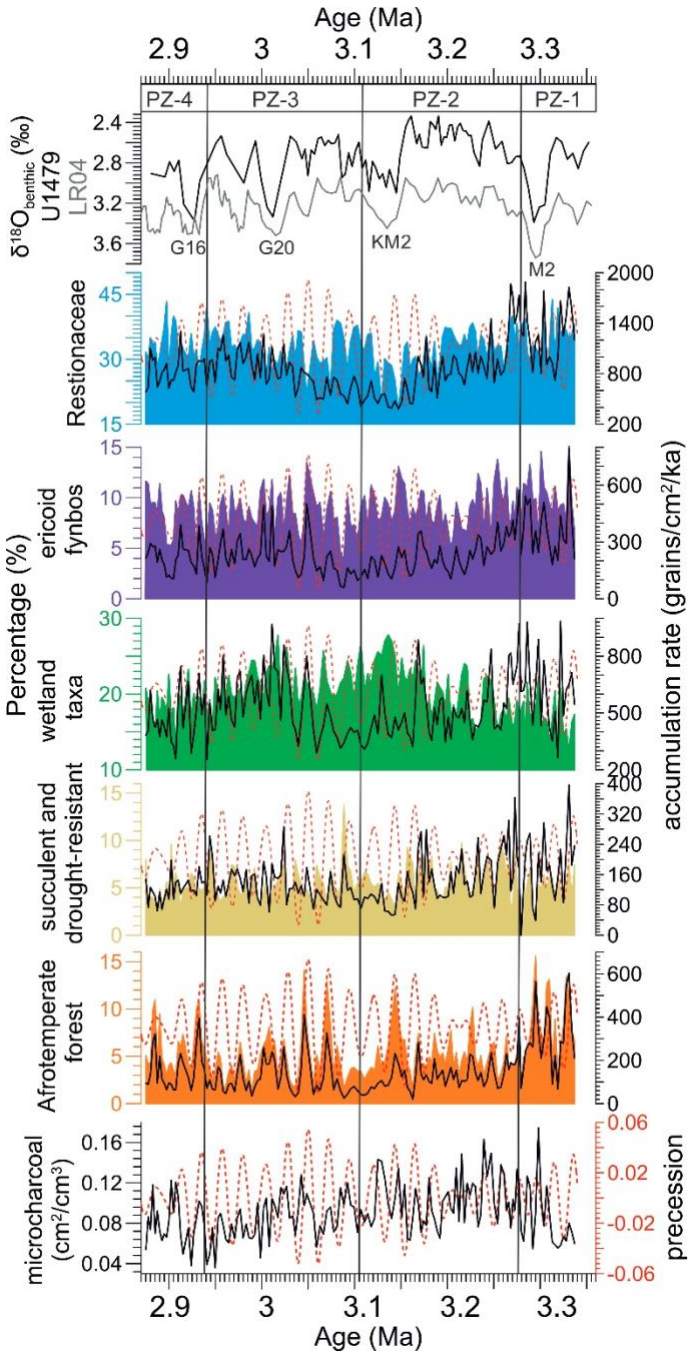

Figure 4. Oxygen isotopes of benthic foraminifera of IODP Site U1479 (black) compared to the global stack LR04 (gray) (Lisiecki and Raymo, 2005), pollen percentages (shading) and accumulation rates (lines) of four groups (Restionaceae, ericoid fynbos, wetland taxa and Afrotemperate forest) as well as the microcharcoal concentrations from IODP Site U1479 overlaid with precession (dashed lines) (Laskar et al., 2004).

The spectral analysis of the Restionaceae, ericoid fynbos, wetland taxa, succulent and drought taxa, and Afrotemperate forest pollen percentages as well as of microcharcoal concentrations show persistent significant power within the 18–24 kyr precession

frequency bands (Figure 5). The same pattern is also found in the frequency analysis of pollen concentrations and accumulation rates (Supplementary Figures 1 and 2).

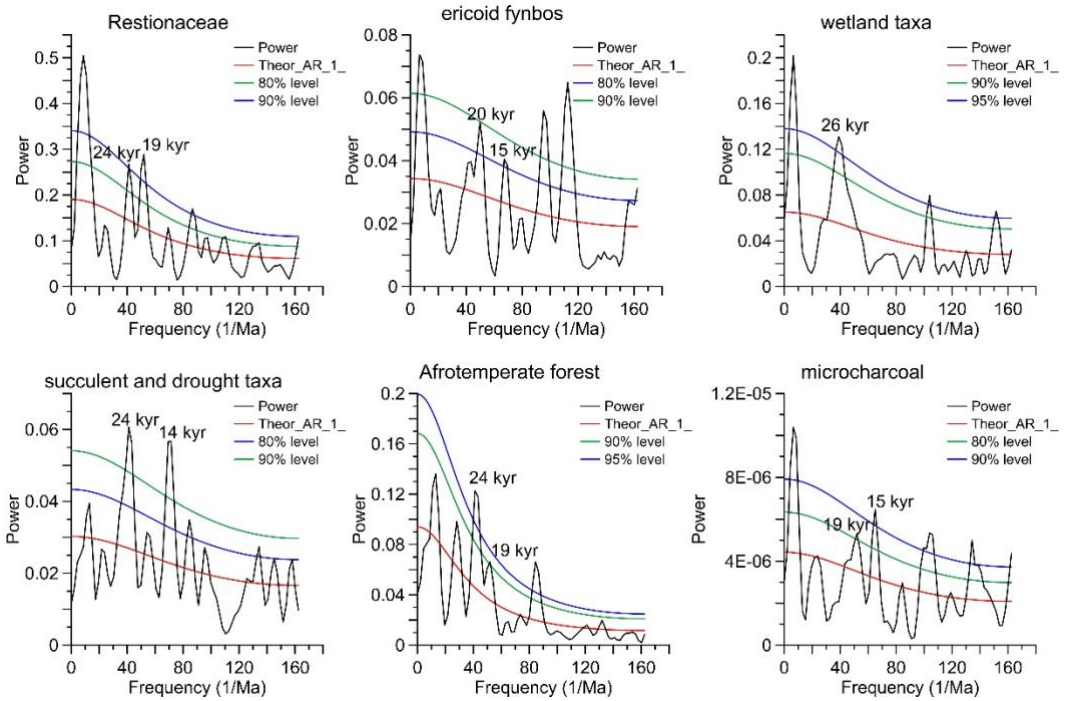

Figure 5. REDFIT spectral analysis (window: hanning; oversample: 2; segments: 3) of the percentages of different pollen groups and microcharcoal concentration from IODP Site U1479. Theor_AR_1_ means theoretical first-order autoregressive (AR1). False-alarm levels of 80%, 90% and 95% are denoted.

The benthic foraminifera $\delta^{18}O$ record shows characteristic 'glacial-interglacial' changes similar to the global LR04 benthic $\delta^{18}O$ stack. The specific values are higher at Site U1479. Several glacials including MIS M2, KM2, G20 and G16 correspond to the minima of Restionaceae and maxima of ericoid fynbos taxa (Figure 6).

5. Discussion

5.1 Pollen transport and source area

Pollen and spores can be transported from the continent to the ocean either by wind or by rivers. Although in the semi-arid regions of southwestern Africa, wind transport is a major transport process for terrigenous material to the ocean (Prospero, 1981; Scott and van Zinderen Barker, 1985), fluvial transport could also be possible. The Pliocene

pollen record at ODP Site 1082 (west of Namibia, Figure 2) indicates mixed fluvial and aeolian pollen transport before 2.2 Ma (Dupont, 2006). Considering that southern South Africa is predominantly influenced by southern westerlies and SE trade winds throughout the year, however, direct wind transport of pollen from the Cape province to Site U1479 seems unlikely as the study site is situated outside the direct influence of the SE trade winds (Figure 2). Pollen and spores in sediments of Site U1479 are more probably transported by the rivers of the Southern Cape in to the ocean and from there by the strong Agulhas Current to the study site. This is supported by the continuous presence of freshwater cyst *Pseudoschizaea* (Rossignol, 1962) in Site U1479 (Figure 3). As previous studies indicate that fine grained, wind-blown terrigenous material can travel as far as the Agulhas Ridge entrained within the Agulhas Current (Petschick et al., 1996), we assume that pollen and spores can also be transported and deposited here. The material of Site U1479 is relatively rich in pollen and spores and the floral composition of the palynological assemblage dominated by the family of Restionaceae clearly points to an origin in fynbos vegetation. We presume, therefore, that the Agulhas Current is instrumental in the westward transport of aeolian or fluvial pollen and spores reaching the ocean along south coast of South Africa.

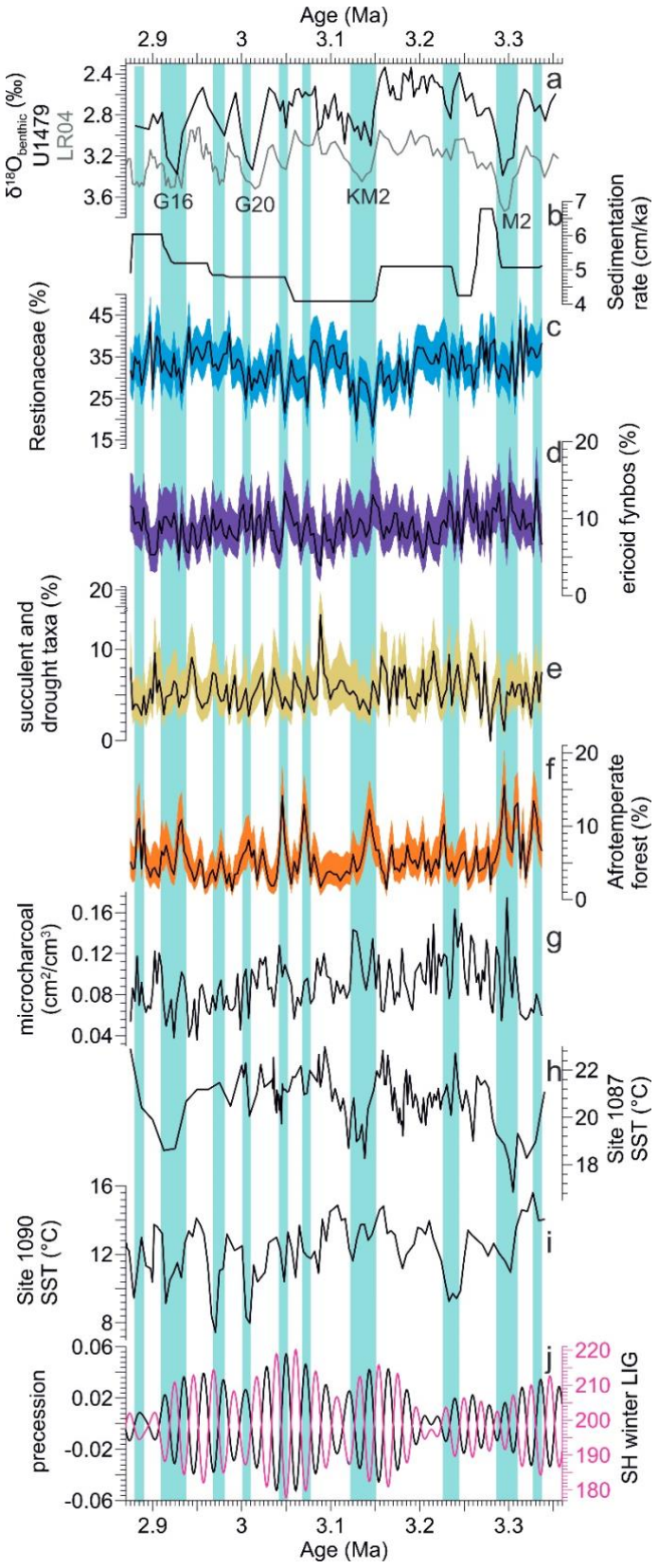

433

434 **Figure 6**. a) Oxygen isotopes of benthic foraminifera of IODP Site U1479 (black) compared to the global
435 stack LR04 (gray) (Lisiecki and Raymo, 2005); b) sedimentation rates, c-f) pollen percentages and g)
436 microcharcoal concentrations of IODP Site U1479; h-i) alkenone-derived SSTs from ODP Sites 1087

(Petrick et al., 2015, 2018) and 1090 (Martínez-García et al., 2010); j) precession (black) and southern hemisphere latitudinal winter insolation gradient (LIG) (pink) (Laskar et al., 2004). Shadings of pollen percentages denote 95% confidence intervals. The light blue vertical bars correspond to higher benthic foraminifera $\delta^{18}O$ values, lower percentages of Restionaceae, high percentages of ericoid fynbos, succulent and drought taxa and Afrotemperate forest, higher values of microcharcoal concentrations in IODP Site U1479 and colder SST in ODP Sites 1087 and 1090.

5.2 Vegetation and hydroclimate response on latitudinal insolation gradient forcing

At IODP Site U1479, the late Pliocene is characterized by a long-term trend of decrease prior to 3.147 Ma and after that an increase of both the percentage values and accumulation rates of Restionaceae correspond to a decrease of Ericaceae values (Figures 4 and 6). The maxima of both Restionaceae and ericoid fynbos taxa before 3.304 Ma indicate that fynbos was the dominant vegetation group in the Cape region, suggesting wetter conditions. However, the general decreasing trend in both percentages and accumulation rates of Restionaceae until 3.147 Ma suggests that that the climate got drier. Pollen accumulation rates depend not only on the production of pollen but also on the transport efficiency. On one hand, drier conditions could result in a decline of vegetation cover leading to less pollen production. On the other hand, it could result in decreased river discharge which might induce less terrestrial input to our core site. This might explain the inverse trend of Cyperaceae, which starts from minima at the beginning of the record and reaches maxima around 3.136 Ma. Cyperaceae growing in wet habitats have an ambiguous relation to wetness. The climate deterioration prior to 3.147 Ma might have caused drying of shallow lakes, which then became wetlands leading to an increase of sedges. The drier conditions are also implied by high microcharcoal concentrations until 3.239 Ma, suggesting an increase in fire under more arid and seasonal conditions and a vegetation providing

463 enough fuel biomass (Daniau et al., 2013). After 3.239 Ma, a further decline of the
464 representation of Restionaceae was observed reaching a minimum at 3.147 Ma; at the
465 same time ericoid fynbos percentages increased to a maximum. This might suggest a
466 shift in the composition of the fynbos. According to Mucina and Rutherford (2006),
467 modern ericoid fynbos is the wettest type of fynbos. However, in this study, the shift to
468 ericoid fynbos appears to be associated with the onset of drier conditions, which is
469 supported by Valsecchi et al. (2013) who propose that ericoid fynbos is favored by drier
470 conditions and higher fire frequencies. The pollen assemblage of the late Pleistocene
471 inferred from the same site (IODP Site U1479) indicates a dramatic decrease in
472 Restionaceae pollen percentages (less than 30%) (unpublished results from Lydie
473 Dupont) in comparison to the pollen assemblage of the middle Pliocene (this study).
474 This suggests the existence of a no-analogue vegetation during the middle Pliocene.
475 The high representation of succulent and drought taxa between 3.273 and 3.156 Ma
476 also indicates relatively dry conditions. At a first glance, this interpretation seems to be
477 inconsistent with the minima in microcharcoal concentrations between 3.195 and 3.154
478 Ma indicating a decrease in fire frequencies. However, fires in southern Africa are
479 affected by the interaction of different factors such as the peak of the dry season, fuel
480 loads and rainfall seasonality (Daniau et al., 2013; Woillez et al., 2014). Additionally,
481 drier conditions resulting in decreased river discharge could also be responsible for
482 less transport of charcoal particles to the ocean. Considering the lower total pollen
483 accumulation rates between 3.239 and 3.059 Ma, the relatively low microcharcoal
484 concentrations are attributed to less fuel biomass and less terrestrial input into ocean.
485 From 3.147 Ma onwards, the increase of Restionaceae pollen percentages
486 accompanied with relatively high wetland taxa percentages, relatively low percentages
487 of ericoid fynbos pollen and succulent and drought taxa indicate a relative increase in
488 humidity.

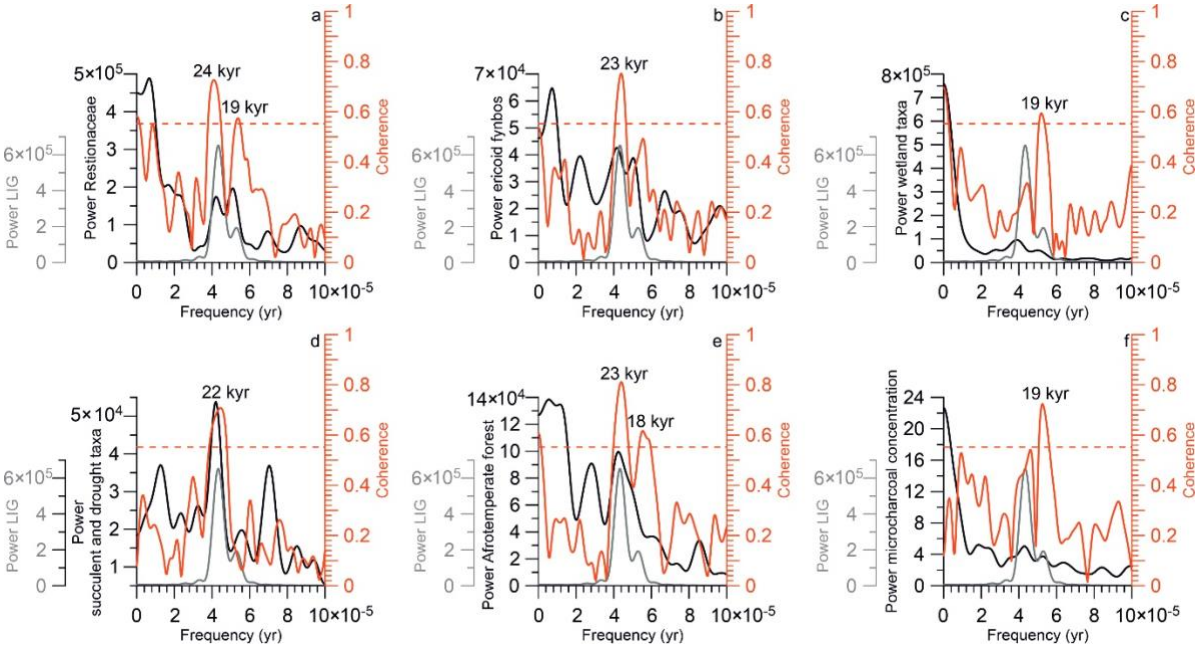

Figure 7. Cross spectral analysis between the percentages of different pollen groups (a, Restionaceae; b, ericoid fynbos; c, wetland taxa; d, succulent and drought taxa; e, Afrotemperate forest) and microcharcoal concentration (f) from IODP Site U1479 and LIG. The dash lines denote the non-zero coherence limit (values higher than 0.55 are significant at the 95% confidence interval).

On orbital and shorter timescales, we find general relationships among the records shown in Figure 6: pollen percentage minima of Restionaceae are associated with maxima of ericoid fynbos, succulent drought taxa, Afrotemperate forest and microcharcoal concentrations. Spectral analysis of the percentage values of Restionaceae, ericoid fynbos, succulent and drought taxa, and Afrotemperate forest as well as microcharcoal concentrations indicates significant periods of 18–24 kyr, suggesting a strong effect of precession (Figure 5). The results of cross spectral analysis support our interpretation indicating significant correlation between pollen groups and LIG at precession cycles (18-24 kyr) (Figure 7). Minima in Restionaceae occur in phase with maxima in precession and minima in LIG between 60 and 30°S of the southern hemisphere winter (21 June) (Supplementary Figure 3). Leads or lags occur in ericoid fynbos (lag of 9500 yr), wetland taxa (lag of 9500 yr), Succulent and

drought taxa (slight lead of 1400 yr), Afrotemperate forest (lead of 9200 yr at 23 kyr cycle and 6100 at 18 kyr cycle) and microcharcoal concentration (lag of 8300 yr).

The dominance of precession cycles in the pollen signal might be the effect of the latitudinal temperature gradient during the southern hemisphere winter approximated by the LIG, which is important in the forcing of the climate in the winter rainfall regions of the mid-latitudes (Davis and Brewer, 2009). A Holocene model climate study shows that a weaker latitudinal temperature gradient leads to weaker mid-latitude westerly flow, weaker cyclones and reduced mid-latitude precipitation (Routson et al., 2019). A reduced equator-to-pole winter temperature gradient was also observed to be related to a reduced equator-to-pole insolation gradient and reduced storm track activity over the Mediterranean Sea using a high-resolution coupled climate mode (Bosmans et al., 2015). A weak southern hemisphere winter gradient would weaken the southern westerlies and reduce winter precipitation in both the WRZ and the YRZ (Figure 8). Restionaceae, which have a strong winter-rainfall affiliation (Cowling et al., 1997), decline due to the relatively dry conditions and reduced rainfall seasonality. Whereas, in comparison to Restionaceae, ericoid fynbos is more favored by drier conditions. Thus, the reduced winter precipitation and less Restionaceae will cause a relative increase of ericoid fynbos. Based on pollen records, we could only refer that the relative abundance of ericoid fynbos is higher which might be resulted from their areal extent. The drier conditions also likely caused higher fire frequencies. The high-resolution marine sediment core MD96-2098 off Namibia during the past 170,000 years in southern Africa indicates high fire activity during precession maxima (Daniau et al., 2013), which is well supported by the microcharcoal-based reconstructions of past fire activity during MIS4 in southern Africa (Woillez et al., 2014). In the YRZ, the high values of Afrotemperate forest suggest more summer rainfall (Dupont et al., 2011; Quick et al., 2018). Conversely a strong gradient would strengthen the westerlies and

associated rainfall in the WRZ and YRZ. Enhanced storm track activity of the southern westerlies would result in humid conditions and intensified rainfall seasonality, leading to high values of Restionaceae and lower values of ericoid fynbos as well as low fire frequencies. A pollen and microcharcoal record from the coastal lake Eilandvlei shows that the general long-term trend of increasing Afrotemperate forest with decreasing fynbos was probably associated with reduced rainfall seasonality and more influences of summer rainfall in maintaining higher moisture availability in the region (Quick et al., 2018). Thus, in the YRZ, the intensified rainfall seasonality and more winter rainfall would hamper the growth of Afrotemperate forest. The pollen record suggests a response of the vegetation to trends in the average winter precipitation by variations in the proportion of Ericaceae in the fynbos. Shifts between the amounts of winter and summer rainfall in the YRZ influenced the development of Afrotemperate forest (Figure 6). In conclusion, we infer that the vegetation variation at the Cape region reflects moisture variability during the mPWP which is related to the LIG in response to precession forcing.

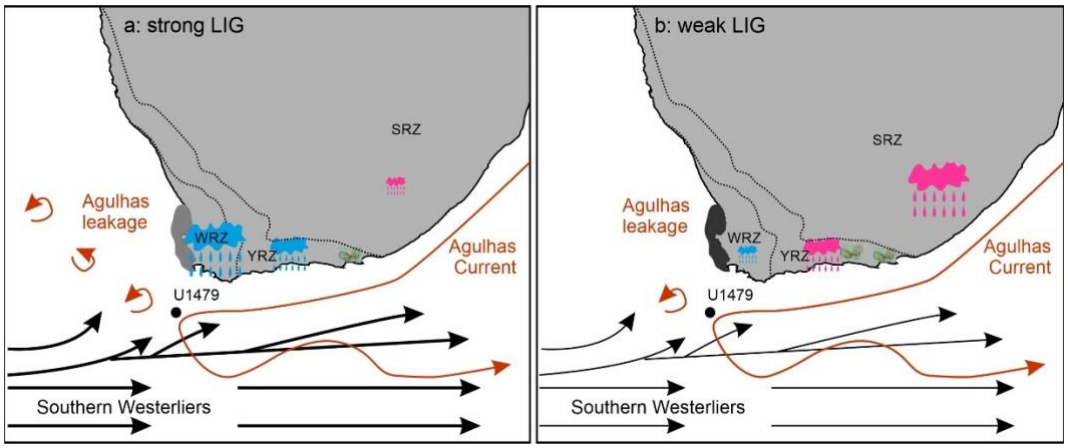

Figure 8. Conceptional model explaining the environmental variability for two different cases during the mPWP in southern Africa. a) strong latitudinal insolation gradient (LIG) inducing strong southern westerlies and warmer SST resulting from Antarctic sea ice retreat, stronger Agulhas leakage and/or weakened upwelling. b) weak LIG inducing weak southern westerlies and cooler SST resulting from Antarctic sea ice expansion, reduced Agulhas leakage and/or strengthened upwelling.

5.3 Vegetation and hydroclimate response during glacials: forcing by sea surface temperatures (SST)

Even within the mPWP there are several glacials. In particular, the pronounced glacial stage just before the onset of the mPWP known as “M2 glaciation” at 3.295 Ma in the global stack LR04 $\delta^{18}O_{benthics}$ record (Lisiecki and Raymo, 2005) has been interpreted as an early major global cooling event prior to the onset of the northern hemisphere glaciations at ca. 2.6 Ma (De Schepper et al., 2009; Prell, 1984). A short interval with lower values of Restionaceae and high values of ericoid fynbos as well as Afrotemperate forest between 3.331 and 3.160 Ma was observed, which is broadly coincident with this glacial MIS M2 (Figure 6). This is supported by the X-ray Fluorescence (XRF) data from IODP Site U1478 off Limpopo which suggest increased runoff during the MIS M2 in the Mozambique Channel probably related to increased rainfall in the SRZ (Koutsodendris et al., 2020). However, the most pronounced period in our pollen record occurs between 3.147 and 3.129 Ma when Restionaceae percentages reach minima together with high values of ericoid fynbos (Figure 6). The period corresponds to another glacial, MIS KM2, which is also considered to be one of the pronounced glacials during the Pliocene (De Schepper et al., 2009). This is supported by the high pollen percentage values of Ericaceae, which are often used as an indicator of colder climate (Gasse and Van Campo, 1998; Scott, 1999). Apart from these two glacials, there are several other glacials characterized by low percentage values of Restionaceae, high percentage values of ericoid fynbos and Afrotemperate forest in our pollen record. The glacials correspond well with cold SST recorded at ODP Sites 1087 and 1090 (Figure 6) (Martínez-García et al., 2010; Petrick et al., 2015, 2018). The TEX_{86} data from IODP Site U1478 off Limpopo also show a long-term SST drop centered at ca. 3.2–3.1 Ma (Taylor et al., in review). We infer that SST influenced

hydroclimate variability and in turn vegetation during the mPWP. The colder SST would reduce temperatures as well as winter rainfall in the WRZ and YRZ, which would lead to a decline in Restionaceae and an increase in ericoid fynbos. The reduced temperature and precipitation in the WRZ of southern Africa would thus enhance the effect of weak winter LIG.

Numerical modelling supports our interpretation. Rreconstructed SST were simulated and used to force a numerical climate model (Kamae et al., 2011). The results reveal that wetter surface conditions in subtropical Africa during the mPWP are related to the reduction of the meridional and zonal gradients of tropical SST rather than to orography, land and/or sea ice. In this region, however, it is hard to distinguish between the different factors resulting in variations of SST, which is affected by the interactions of Agulhas leakage, Benguela Current as well as the advection of cold sub-Antarctic water (Rosell-Melé et al., 2014).

Firstly, a decline in SST might be attributed to the global cooling triggered by Antarctic ice sheet expansion. Proxy records and model studies generally infer a more northward position of the southern westerlies during cooler climates/glacial periods (Bard and Rickaby, 2009; Lamy et al., 2004; Williams and Bryan, 2006). A 800,000 year record of SST and ocean productivity from marine sediment core MD96-2077 situated under the Agulhas Current of the subtropical gyre of the Indian Ocean suggests a northward shift of the southern westerlies by up to 7° of latitude during cooler stages (Bard and Rickaby, 2009). This supports the model results of a 7° equatorward shift of the subtropical fronts resulting from a global cooling of 3°C (Williams and Bryan, 2006). The inference of weakened southern westerlies induced by the weak LIG during glacials based on our pollen and microcharcoal records implies that there might be some decoupling between the strength and the latitudinal position of the southern

603 westerlies. During glacials, northerly positioned southern westerlies might still show
604 fluctuations in strength.

605 Secondly, a decline in SST might be attributed to less Agulhas leakage. Previous
606 studies have shown that the northward shift of the southern westerlies during glacials
607 nearly shuts off the Agulhas leakage (Bard and Rickaby, 2009; Peeters et al., 2004).
608 The initial results of geochemical provenance studies on clays at our Site U1479
609 indicate reduced Agulhas leakage during the last glacial cycle and enhanced Agulhas
610 leakage during warmer periods (Franzese et al., 2018). The reconstructions of ice
611 sheet, SST and sea ice from an Antarctic sediment core showed that the intensification
612 of Antarctic cooling resulted in the expansion of southern westerlies and the northward
613 migration of ocean fronts in the Southern Ocean, which likely restricted the warm
614 Agulhas leakage (McKay et al., 2012). In this case, the low SST might be associated
615 with less Agulhas leakage influenced by the northward shift and weakened southern
616 westerlies during weak LIG. This is supported by the relatively cool SST and very low
617 abundances of Agulhas leakage indicator foraminifera (e.g., *Globigerina falconensis*
618 and *Globorotalia menardii*) at ODP Site 1087 suggesting an absence or weak influence
619 of Agulhas leakage during the mPWP (Petrick et al., 2015). The high representation of
620 Podocarpaceae during glacials in combination with restricted Agulhas leakage refutes
621 the idea of abundant Podocarpaceae pollen transport by the Agulhas Current from
622 southeastern South Africa. More likely, therefore, is that abundant pollen of
623 Podocarpaceae originated from Afrotemperate forest in the YRZ. Although it is widely
624 accepted that the southward shift of the southern westerlies would enable more
625 Agulhas leakage (Biastoch et al., 2009), the modeling study of Durgadoo et al. (2013)
626 emphasized that increased Agulhas leakage corresponds with increased intensity of
627 the southern westerlies, which would concur with our "strong LIG" case shown in
628 Figure 8.

Thirdly, a decline in SST might mark the switch from a warm to a cold mode of SE trade wind-induced upwelling along the southwest African coast. Grain size data and alkenone-based SST from sediment cores MD96-2086/87 located off Lüderitz (off Namibia, SW Africa) indicate that the past long-term SST variations are primarily induced by strengthened SE trade winds through intensified coastal upwelling (Pichevin et al., 2005). The latest model results indicate intensification of upwelling of colder waters in the Benguela Upwelling region during the Pleistocene resulting in strongly lowered SST compared to the Pliocene, which is not simulated by global models with a relatively coarse geographical resolution (Jung et al., 2014; Haywood et al., 2020, accepted; McClymont et al., 2020). Although the upwelling was still weak during the middle Pliocene, several studies have shown evidence of an upwelling maximum in the southern Benguela system until ca. 2.8 Ma, which later progressed northwards to its modern position offshore Lüderitz (Diekmann et al., 2003; Petrick et al., 2015, 2018; Rommerskirchen et al., 2011). Fossil mollusc records from the west coast of southern Africa indicate the existence of cold upwelling offshore south of 32°S in the early Pleistocene (Tankard and Rogers, 1978). Alkenone-derived SST records from the Agulhas Basin to the northern Benguela system indicate different patterns of SST since 5 Ma (Etourneau et al., 2009; Martínez-García et al., 2010; Petrick et al., 2015, 2018; Rommerskirchen et al., 2011; Rosell-Melé et al., 2014), suggesting upwelling was controlled by different processes in the southern and northern Benguela system. This is for instance supported by the absence of cold SST in the northern Benguela system (ODP Sites1084, 1082 and 1081) during the glacials MIS M2 and KM2 (Petrick et al., 2015). Multiproxy studies suggest more extensive upwelling in the southern Benguela system during the mPWP (Petrick et al., 2015). The global cooling with increased Antarctic glaciations promoting intermediate and bottom water formation combined with intensified SE trade winds (intensified Hadley circulation) and

uplift of East Africa would have caused intensified upwelling offshore of southern Africa (Etourneau et al., 2009; Jung et al., 2014; Marlow et al., 2000; Rommerskirchen et al., 2011; Rosell-Melé et al., 2014). In our "weak LIG" case, the weakened southern westerlies combined with strong SE trade winds would cause intensified upwelling, resulting in cold water conditions over our core site and less rainfall in the WRZ. Whereas in the "strong LIG" case, the strong southern westerlies and weak SE trade winds would cause weakened upwelling (Figure 8).

6 Conclusions

The development of vegetation and climate in southwestern South Africa during the mid-Piacenzian have been documented in detail by pollen, microcharcoal and benthic foraminifera oxygen isotope records from marine sediment cores of IODP Site U1479 retrieved from the Cape Basin offshore of South Africa covering the period from 3.337 to 2.875 Ma.

Pollen assemblages throughout the record are characterized by the family of Restionaceae indicating a clear pollen source from fynbos vegetation during the mPWP. Variations in the representation of Restionaceae, ericoid fynbos and Afrotemperate forest show dominant precession cycles indicating influence by the latitudinal insolation gradient (LIG) in response to precession forcing. The weak/strong southern hemisphere winter gradient would weaken/strengthen the southern westerlies and winter precipitation in the WRZ and YRZ as well as influence the relative amounts between winter and summer rainfall in the YRZ.

The glacial events reflected by the benthic foraminifera oxygen isotope record correspond well with cooler SE Atlantic sea surface temperatures (SST) off South Africa and are consistent with the vegetation and hydroclimate variability deduced from our pollen and microcharcoal records. The cooler SST inducing less rainfall in the

winter rainfall zone, were likely driven by interactions of both atmospheric and oceanographic processes including Antarctic ice sheet expansion, less contribution of the Agulhas leakage and/or intensified southern Benguela upwelling.

On the basis of our study and comparisons with published records offshore of southwestern Africa, we propose that LIG forcing (precession) and SST forcing were the main drivers of hydroclimate in southwestern South Africa during the mPWP. During “weak LIG”, the weakened southern westerlies combined with cold SST result in less rainfall in the WRZ, while during “strong LIG”, the strong southern westerlies together with warm SST would bring more rainfall in the WRZ.

Acknowledgments

This study was financially supported by the International Ocean Discovery Program, IODP (SPP527) of the Deutsche Forschungsgemeinschaft (DFG), grant Nr. DU221/7. Thibaut Caley is supported by CNRS-INSU. Funding from IODP France and LEFE IMAGO CNRS INSU project SeaSalt are acknowledged. We thank the Captain, officers, crew and especially all scientists sailing on IODP expedition 361. Thanks to Jutta Scheffing for assistance with the pollen sample preparations in the lab. We would like to thank the two reviewers for their helpful and constructive comments that have helped to improve the manuscript.

References

Bard, E., Rickaby, R.E., 2009. Migration of the subtropical front as a modulator of glacial climate. Nature 460, 380-383, https://doi.org/10.1038/nature08189.

Bergh, N.G., Verboom, G., Rouget, M., Cowling, R.M., 2014. Vegetation types of the greater cape floristic region, in: Allsopp, N., Colville, J.F., Verboom, G.A. (Eds.), Fynbos: Ecology, evolution, and conservation of a megadiverse region. Oxford University Press. https://doi.org/10.1093/acprof:oso/9780199679584.003.0001.

Biastoch, A., Böning, C.W., Schwarzkopf, F.U., Lutjeharms, J., 2009. Increase in Agulhas leakage due to poleward shift of Southern Hemisphere westerlies. Nature 462, 495-498, https://doi.org/10.1038/nature08519.

Bond, W., 1996. Fire, in: Cowling, R., Richardson, D., Pierce, S. (Eds.), The vegetation of southern Africa. Cambridge University Press: Cambridge, pp. 421-446.

Bonnefille, R., Riollet, G., 1980. Pollen des savanes d'Afrique orientale. Éditions du Centre national de la recherche scientifique, Paris.

Bosmans, J., Drijfhout, S., Tuenter, E., Hilgen, F., Lourens, L.J., Rohling, E., 2015. Precession and obliquity forcing of the freshwater budget over the Mediterranean. Quaternary Science Reviews 123, 16-30, http://dx.doi.org/10.1016/j.quascirev.2015.06.008.

Burls, N.J., Fedorov, A.V., 2017. Wetter subtropics in a warmer world: Contrasting past and future hydrological cycles. Proceedings of the National Academy of Sciences 114, 12888-12893, https://doi.org/10.1073/pnas.1703421114.

Carr, A.S., Boom, A., Grimes, H.L., Chase, B.M., Meadows, M.E., Harris, A., 2014. Leaf wax n-alkane distributions in arid zone South African flora: Environmental controls, chemotaxonomy and palaeoecological implications. Organic Geochemistry 67, 72-84, https://doi.org/10.1016/j.orggeochem.2013.12.004.

Chase, B.M., Meadows, M.E., 2007. Late Quaternary dynamics of southern Africa's winter rainfall zone. Earth-Science Reviews 84, 103-138, https://doi.org/10.1016/j.earscirev.2007.06.002.

Clark, R.L., 1982. Point count estimation of charcoal in pollen preparations and thin sections of sediments. Pollen et spores 24, 23-35.

Cowling, R.M., Richardson, D.M., Pierce, S.M., 1997. Vegetation of southern Africa. Cambridge University Press, Cambridge.

Crowley, T.J., 1996. Pliocene climates: the nature of the problem. Marine Micropaleontology 27, 3-12, https://doi.org/10.1016/0377-8398(95)00049-6.

Daniau, A.-L., Sánchez Goñi, M.F., Martinez, P., Urrego, D.H., Bout-Roumazeilles, V., Desprat, S., Marlon, J.R., 2013. Orbital-scale climate forcing of grassland burning in southern

733 Africa. Proceedings of the National Academy of Sciences 110, 5069-5073,
734 https://doi.org/10.1073/pnas.1214292110.
735 Davis, B.A.S., Brewer, S., 2009. Orbital forcing and role of the latitudinal insolation/temperature
736 gradient. Climate Dynamics 32, 143-165, https://doi.org/10.1007/s00382-008-0480-9.
737 De Schepper, S., Head, M.J., Groeneveld, J., 2009. North Atlantic Current variability through
738 marine isotope stage M2 (circa 3.3 Ma) during the mid-Pliocene. Paleoceanography 24,
739 https://doi.org/10.1029/2008pa001725.
740 Diekmann, B., Fälker, M., Kuhn, G., 2003. Environmental history of the south-eastern South
741 Atlantic since the Middle Miocene: evidence from the sedimentological records of ODP
742 Sites 1088 and 1092. Sedimentology 50, 511-529, https://doi.org/10.1046/j.1365-
743 3091.2003.00562.x.
744 Dolan, A.M., Haywood, A.M., Hill, D.J., Dowsett, H.J., Hunter, S.J., Lunt, D.J., Pickering, S.J.,
745 2011. Sensitivity of Pliocene ice sheets to orbital forcing. Palaeogeography,
746 Palaeoclimatology, Palaeoecology 309, 98-110,
747 https://doi.org/10.1016/j.palaeo.2011.03.030.
748 Dowsett, H.J., Cronin, T.M., Poore, R.Z., Thompson, R.S., Whatley, R.C., Wood, A.M., 1992.
749 Micropaleontological Evidence for Increased Meridional Heat Transport in the North
750 Atlantic Ocean During the Pliocene. Science 258, 1133-1135.
751 https://doi.org/10.1126/science.258.5085.1133.
752 Dupont, L.M., 2006. Late Pliocene vegetation and climate in Namibia (southern Africa) derived
753 from palynology of ODP Site 1082. Geochemistry, Geophysics, Geosystems 7,
754 https://doi.org/10.1029/2005gc001208.
755 Dupont, L.M., Linder, H.P., Rommerskirchen, F., Schefuß, E., 2011. Climate-driven rampant
756 speciation of the Cape flora. Journal of Biogeography 38, 1059-1068,
757 https://doi.org/10.1111/j.1365-2699.2011.02476.x.
758 Durgadoo, J.V., Loveday, B.R., Reason, C.J., Penven, P., Biastoch, A., 2013. Agulhas leakage
759 predominantly responds to the Southern Hemisphere westerlies. Journal of Physical
760 Oceanography 43, 2113-2131, https://doi.org/10.1175/JPO-D-13-047.1.

761 Eckardt, F., Kuring, N., 2005. SeaWiFS identifies dust sources in the Namib Desert.
762 International Journal of Remote Sensing 26, 4159-4167,
763 https://doi.org/10.1080/01431160500113112.
764 Engelbrecht, C.J., Landman, W.A., Engelbrecht, F.A., Malherbe, J., 2015. A synoptic
765 decomposition of rainfall over the Cape south coast of South Africa. Climate Dynamics
766 44, 2589-2607, https://doi.org/10.1007/s00382-014-2230-5.
767 Etourneau, J., Martinez, P., Blanz, T., Schneider, R., 2009. Pliocene–Pleistocene variability of
768 upwelling activity, productivity, and nutrient cycling in the Benguela region. Geology 37,
769 871-874, https://doi.org/10.1130/g25733a.1.
770 Franzese, A.M., Hemming, S.R., Pearson, B., Kafando, O., Sinadinse, A., 2018. Assessing
771 Agulhas Leakage using Terrigenous Sediment Provenance at IODP Site U1479: Initial
772 Results, AGU Fall Meeting Abstracts.
773 Gasse, F., Van Campo, E., 1998. A 40,000-yr pollen and diatom record from Lake Tritrivakely,
774 Madagascar, in the southern tropics. Quaternary Research 49, 299-311,
775 https://doi.org/10.1006/qres.1998.1967.
776 Goldblatt, P., Manning, J.C., 2002. Plant diversity of the Cape region of southern Africa. Annals
777 of the Missouri Botanical Garden, 281-302, https://doi.org/10.2307/3298566.
778 Grimm, E., 2015. Tilia and TGView 19 version 2.0. 41. software. Springfield, USA: Illinois State
779 Museum, Research and Collection Center.
780 Hall, I., Hemming, S., LeVay, L., Barker, S., Berke, M., Brentegani, L., Caley, T., Cartagena-
781 Sierra, A., Charles, C., Coenen, J., 2017. Site U1479, Proceedings of the International
782 Ocean Discovery Program, 361. International Ocean Discovery Program.
783 Hammer, Ø., Harper, D.A., Ryan, P.D., 2001. PAST: Paleontological statistics software
784 package for education and data analysis. Palaeontologia electronica 4, 9.
785 Haywood, A.M., Dowsett, H.J., Valdes, P.J., Lunt, D.J., Francis, J.E., Sellwood, B.W., 2009.
786 Introduction. Pliocene climate, processes and problems. Philosophical Transactions of
787 the Royal Society A: Mathematical, Physical and Engineering Sciences 367, 3-17,
788 https://doi.org/10.1098/rsta.2008.0205.

Haywood, A.M., Hill, D.J., Dolan, A.M., Otto-Bliesner, B.L., Bragg, F., Chan, W.L., Chandler, M.A., Contoux, C., Dowsett, H.J., Jost, A., Kamae, Y., Lohmann, G., Lunt, D.J., Abe-Ouchi, A., Pickering, S.J., Ramstein, G., Rosenbloom, N.A., Salzmann, U., Sohl, L., Stepanek, C., Ueda, H., Yan, Q., Zhang, Z., 2013. Large-scale features of Pliocene climate: results from the Pliocene Model Intercomparison Project. Climate of the Past 9, 191-209, https://doi.org/10.5194/cp-9-191-2013.

Haywood, A.M., Tindall, J.C., Dowsett, H.J., Dolan, A.M., Foley, K.M., Hunter, S.J., Hill, D.J., Chan, W.L., Abe-Ouchi, A., Stepanek, C., Lohmann, G., Chandan, D., Peltier, W.R., Tan, N., Contoux, C., Ramstein, G., Li, X., Zhang, Z., Guo, C., Nisancioglu, K.H., Zhang, Q., Li, Q., Kamae, Y., Chandler, M.A., Sohl, L.E., Otto-Bliesner, B.L., Feng, R., Brady, E.C., von der Heydt, A.S., Baatsen, M.L.J., Lunt, D.J., 2020. A return to large-scale features of Pliocene climate: the Pliocene Model Intercomparison Project Phase 2. Climate of the Past Discuss. 2020, 1-40, https://doi.org/10.5194/cp-2019-145.

Haywood, A.M., Valdes, P.J., 2004. Modelling Pliocene warmth: contribution of atmosphere, oceans and cryosphere. Earth and Planetary Science Letters 218, 363-377, https://doi.org/10.1016/S0012-821X(03)00685-X.

Hijmans, R., Cameron, S., Parra, J., Jones, P., Jarvis, A., Richardson, K., 2005. WorldClim, version 1.3, University of California, Berkeley.

Hunter, S.J., Haywood, A.M., Dolan, A.M., Tindall, J.C., 2019. The HadCM3 contribution to PlioMIP phase 2. Climate of the Past 15, 1691-1713, https://doi.org/10.5194/cp-15-1691-2019.

Jung, G., Prange, M., Schulz, M., 2014. Uplift of Africa as a potential cause for Neogene intensification of the Benguela upwelling system. Nature Geoscience 7, 741-747, https://doi.org/10.1038/ngeo2249.

Kamae, Y., Ueda, H., Kitoh, A., 2011. Hadley and Walker circulations in the mid-Pliocene warm period simulated by an atmospheric general circulation model. Journal of the Meteorological Society of Japan. Ser. II 89, 475-493, https://doi.org/10.2151/jmsj.2011-505.

817 Koutsodendris, A., Nakajima, K., Kaboth-Bahr, S., Berke, M.A., Franzese, A.M., Hall, I.R.,
818 Hemming, S.R., Just, J., LeVay, L.J., Pross, J., Robinson, R., and IODP Expedition 361
819 scientists, 2020: A Plio-Pleistocene (c. 0 – 4 Ma) cyclostratigraphy for IODP Site U1478
820 (Mozambique Channel, SW Indian Ocean): Exploring an offshore record of
821 paleoclimate and ecosystem variability in SE Africa. Newsletters on Stratigraphy,
822 https://doi.org/10.1127/nos/2020/0608.
823 Lamy, F., Kaiser, J., Ninnemann, U., Hebbeln, D., Arz, H.W., Stoner, J., 2004. Antarctic timing
824 of surface water changes off Chile and Patagonian ice sheet response. Science 304,
825 1959-1962, https://doi.org/10.1126/science.1097863.
826 Laskar, J., Robutel, P., Joutel, F., Gastineau, M., Correia, A.C.M., Levrard, B., 2004. A long-
827 term numerical solution for the insolation quantities of the Earth. A&A 428, 261-285,
828 https://doi.org/10.1051/0004-6361:20041335.
829 Lau, W.K.M., Wu, H.T., Kim, K.M., 2013. A canonical response of precipitation characteristics
830 to global warming from CMIP5 models. Geophysical Research Letters 40, 3163-3169,
831 https://doi.org/10.1002/grl.50420.
832 Levin, N.E., 2015. Environment and climate of early human evolution. Annual Review of Earth
833 and Planetary Sciences 43, 405-429, https://doi.org/10.1146/annurev-earth-060614-
834 105310.
835 Linder, H.P., 2003. The radiation of the Cape flora, southern Africa. Biological Reviews 78,
836 597-638, https://doi.org/10.1017/s1464793103006171.
837 Lisiecki, L.E., Raymo, M.E., 2005. A Pliocene-Pleistocene stack of 57 globally distributed
838 benthic δ18O records. Paleoceanography 20, https://doi.org/10.1029/2004pa001071.
839 Lunt, D.J., Haywood, A.M., Schmidt, G.A., Salzmann, U., Valdes, P.J., Dowsett, H.J., Loptson,
840 C.A., 2012. On the causes of mid-Pliocene warmth and polar amplification. Earth and
841 Planetary Science Letters 321, 128-138, https://doi.org/10.1016/j.epsl.2011.12.042.
842 Maher, L.J., 1972. Nomograms for computing 0.95 confidence limits of pollen data. Review of
843 Palaeobotany and Palynology 13, 85-93, http://dx.doi.org/10.1016/0034-
844 6667(72)90038-3.

Marchitto, T., Curry, W., Lynch-Stieglitz, J., Bryan, S., Cobb, K., Lund, D., 2014. Improved oxygen isotope temperature calibrations for cosmopolitan benthic foraminifera. Geochimica et Cosmochimica Acta 130, 1-11, https://doi.org/10.1016/j.gca.2013.12.034.

Martin, H., 2006. Cenozoic climatic change and the development of the arid vegetation in Australia. Journal of Arid Environments 66, 533-563, https://doi.org/10.1016/j.jaridenv.2006.01.009.

Martínez-García, A., Rosell-Melé, A., McClymont, E.L., Gersonde, R., Haug, G.H., 2010. Subpolar Link to the Emergence of the Modern Equatorial Pacific Cold Tongue. Science 328, 1550-1553, https://doi.org/10.1126/science.1184480.

McClymont, E.L., Ford, H.L., Ho, S.L., Tindall, J.C., Haywood, A.M., Alonso-Garcia, M., Bailey, I., Berke, M.A., Littler, K., Patterson, M.O., Petrick, B., Peterse, F., Ravelo, A.C., Risebrobakken, B., De Schepper, S., Swann, G.E.A., Thirumalai, K., Tierney, J.E., van der Weijst, C., White, S., Abe-Ouchi, A., Baatsen, M.L.J., Brady, E.C., Chan, W.L., Chandan, D., Feng, R., Guo, C., von der Heydt, A.S., Hunter, S., Li, X., Lohmann, G., Nisancioglu, K.H., Otto-Bliesner, B.L., Peltier, W.R., Stepanek, C., Zhang, Z., 2020. Lessons from a high-CO2 world: an ocean view from ~ 3 million years ago. Climate of the Past 16, 1599-1615, https://doi.org/10.5194/cp-16-1599-2020.

McKay, R., Naish, T., Carter, L., Riesselman, C., Dunbar, R., Sjunneskog, C., Winter, D., Sangiorgi, F., Warren, C., Pagani, M., Schouten, S., Willmott, V., Levy, R., DeConto, R., Powell, R.D., 2012. Antarctic and Southern Ocean influences on Late Pliocene global cooling. Proceedings of the National Academy of Sciences 109, 6423-6428, https://doi.org/10.1073/pnas.1112248109.

Mucina, L., Rutherford, M.C., 2006. The Vegetation of South Africa, Lesotho and Swaziland. South African National Biodiversity Institute.

Nelson, G., Hutchings, L., 1983. The Benguela upwelling area. Progress in Oceanography 12, 333-356, http://dx.doi.org/10.1016/0079-6611(83)90013-7.

Pagani, M., Liu, Z., LaRiviere, J., Ravelo, A.C., 2010. High Earth-system climate sensitivity determined from Pliocene carbon dioxide concentrations. Nature Geoscience 3, 27-30, https://doi.org/10.1038/ngeo724.

Paillard, D., Labeyrie, L., Yiou, P., 1996. AnalySeries 1.0: a Macintosh software for the analysis of geophysical time-series. Eos 77, 379.

Peeters, F.J.C., Acheson, R., Brummer, G.-J.A., de Ruijter, W.P.M., Schneider, R.R., Ganssen, G.M., Ufkes, E., Kroon, D., 2004. Vigorous exchange between the Indian and Atlantic oceans at the end of the past five glacial periods. Nature 430, 661-665, http://dx.doi.org/10.1038/nature02785.

Petrick, B., McClymont, E.L., Felder, S., Rueda, G., Leng, M.J., Rosell-Melé, A., 2015. Late Pliocene upwelling in the Southern Benguela region. Palaeogeography, Palaeoclimatology, Palaeoecology 429, 62-71, https://doi.org/10.1016/j.palaeo.2015.03.042.

Petrick, B., McClymont, E.L., Littler, K., Rosell-Melé, A., Clarkson, M.O., Maslin, M., Röhl, U., Shevenell, A.E., Pancost, R.D., 2018. Oceanographic and climatic evolution of the southeastern subtropical Atlantic over the last 3.5 Ma. Earth and Planetary Science Letters 492, 12-21, https://doi.org/10.1016/j.epsl.2018.03.054.

Petschick, R., Kuhn, G., Gingele, F., 1996. Clay mineral distribution in surface sediments of the South Atlantic: sources, transport, and relation to oceanography. Marine Geology 130, 203-229, https://doi.org/10.1016/0025-3227(95)00148-4.

Pichevin, L., Cremer, M., Giraudeau, J., Bertrand, P., 2005. A 190 ky record of lithogenic grain-size on the Namibian slope: Forging a tight link between past wind-strength and coastal upwelling dynamics. Marine Geology 218, 81-96, https://doi.org/10.1016/j.margeo.2005.04.003.

Prell, W.L., 1984. Covariance Patterns of Foraminiferal δ18O: An Evaluation of Pliocene Ice Volume Changes Near 3.2 Million Years Ago. Science 226, 692-694, https://doi.org/10.1126/science.226.4675.692.

899 Prescott, C.L., Dolan, A.M., Haywood, A.M., Hunter, S.J., Tindall, J.C., 2018. Regional climate
900 and vegetation response to orbital forcing within the mid-Pliocene Warm Period: A
901 study using HadCM3. Global and Planetary Change 161, 231-243,
902 https://doi.org/10.1016/j.gloplacha.2017.12.015.
903 Prospero, J., 1981. Aeolian transport to the world ocean, in: Emiliani, C. (Ed.), The sea, vol. 7,
904 The oceanic lithosphere. Wiley Interscience, New York, pp. 801-874.
905 Quick, L.J., Chase, B.M., Wündsch, M., Kirsten, K.L., Chevalier, M., Mäusbacher, R.,
906 Meadows, M.E., Haberzettl, T., 2018. A high-resolution record of Holocene climate and
907 vegetation dynamics from the southern Cape coast of South Africa: pollen and
908 microcharcoal evidence from Eilandvlei. Journal of Quaternary Science 33, 487-500,
909 https://doi.org/10.1002/jqs.3028.
910 Raymo, M.E., Grant, B., Horowitz, M., Rau, G.H., 1996. Mid-Pliocene warmth: stronger
911 greenhouse and stronger conveyor. Marine Micropaleontology 27, 313-326,
912 https://doi.org/10.1016/0377-8398(95)00048-8.
913 Raymo, M.E., Mitrovica, J.X., O'Leary, M.J., DeConto, R.M., Hearty, P.J., 2011. Departures
914 from eustasy in Pliocene sea-level records. Nature Geoscience 4, 328-332,
915 https://doi.org/10.1038/ngeo1118.
916 Rind, D., Chandler, M., 1991. Increased ocean heat transports and warmer climate. Journal of
917 Geophysical Research: Atmospheres 96, 7437-7461.
918 https://doi.org/10.1029/91jd00009.
919 Rommerskirchen, F., Condon, T., Mollenhauer, G., Dupont, L., Schefuss, E., 2011. Miocene
920 to Pliocene development of surface and subsurface temperatures in the Benguela
921 Current system. Paleoceanography 26, https://doi.org/10.1029/2010pa002074.
922 Rosell-Melé, A., Martínez-Garcia, A., McClymont, E.L., 2014. Persistent warmth across the
923 Benguela upwelling system during the Pliocene epoch. Earth and Planetary Science
924 Letters 386, 10-20, https://doi.org/10.1016/j.epsl.2013.10.041.
925 Rossignol, M., 1962. Analyse pollinique de sédiments marins quaternaires en Israël II. -
926 Sédiments pleistocènes. Pollen et Spores 4, 121-148.

927 Routson, C.C., McKay, N.P., Kaufman, D.S., Erb, M.P., Goosse, H., Shuman, B.N., Rodysill,
928 J.R., Ault, T., 2019. Mid-latitude net precipitation decreased with Arctic warming during
929 the Holocene. Nature 568, 83-87, https://doi.org/10.1038/s41586-019-1060-3.
930 Salzmann, U., Haywood, A.M., Lunt, D.J., Valdes, P.J., Hill, D.J., 2008. A new global biome
931 reconstruction and data-model comparison for the Middle Pliocene. Global Ecology and
932 Biogeography 17, 432-447, https://doi.org/10.1111/j.1466-8238.2008.00381.x.
933 Schulz, M., Mudelsee, M., 2002. REDFIT: estimating red-noise spectra directly from unevenly
934 spaced paleoclimatic time series. Computers & Geosciences 28, 421-426,
935 https://doi.org/10.1016/S0098-3004(01)00044-9.
936 Scott, L., 1982. Late Quaternary fossil pollen grains from the Transvaal, South Africa. Review
937 of Palaeobotany and Palynology 36, 241-278, https://doi.org/10.1016/0034-
938 6667(82)90022-7.
939 Scott, L., 1999. Vegetation history and climate in the Savanna biome South Africa since
940 190,000 ka: a comparison of pollen data from the Tswaing Crater (the Pretoria Saltpan)
941 and Wonderkrater. Quaternary International 57, 215-223,
942 https://doi.org/10.1016/S1040-6182(98)00062-7.
943 Scott, L., Partridge, T., 1994. Some manifestations of Pliocene warming in southern Africa, in:
944 Thompson, R.S. (Ed.), Pliocene Terrestrial Environments and Data/Model
945 Comparisons. US Geological Survey Open-File Report 94-23, pp. 54-55.
946 Scott, L., van Zinderen Barker, S.E., 1985. Exotic pollen and long-distance wind dispersal at a
947 sub-Antarctic Island. Grana 24, 45-54. https://doi.org/10.1080/00173138509427422.
948 Shannon, L.V., Nelson, G., 1996. The Benguela: large scale features and processes and
949 system variability, in: Wefer, G., Berger, W.H., Siedler, G., Webb, D. (Eds.), The South
950 Atlantic: Present and Past Circulation. Springer-Verlag, Berlin Heidelberg, pp. 63-210.
951 Tankard, A.J., Rogers, J., 1978. Late Cenozoic Palaeoenvironments on the West Coast of
952 Southern Africa. Journal of Biogeography 5, 319-337, https://doi.org/10.2307/3038026.
953 Tyson, P.D., Preston-Whyte, R.A., 2000. The weather and climate of southern Africa. Oxford
954 University Press, Cape Town.

Valsecchi, V., Chase, B.M., Slingsby, J.A., Carr, A.S., Quick, L.J., Meadows, M.E., Cheddadi, R., Reimer, P.J., 2013. A high resolution 15,600-year pollen and microcharcoal record from the Cederberg Mountains, South Africa. Palaeogeography, Palaeoclimatology, Palaeoecology 387, 6-16, https://doi.org/10.1016/j.palaeo.2013.07.009.

Van As, J., du Preez, J., Brown, L., Smit, N., 2012. The Story of Life & the Environment. Penguin Random House South Africa.

Wheeler, A.D., 2010. Impacts of degradation on critically endangered Oudtshoorn Gannaveld. University of the Western Cape, Cape Town, South Africa.

Williams, G.P., Bryan, K., 2006. Ice age winds: An aquaplanet model. Journal of climate 19, 1706-1715, https://doi.org/10.1175/JCLI3766.1.

Woillez, M.-N., Levavasseur, G., Daniau, A.-L., Kageyama, M., Urrego, D., Sánchez-Goñi, M.-F., Hanquiez, V., 2014. Impact of precession on the climate, vegetation and fire activity in southern Africa during MIS4. Climate of the Past 10, 1165-1182, https://doi.org/10.5194/cp-10-1165-2014.

Zhao, X., Dupont, L., Meadows, M.E., Wefer, G., 2016a. Pollen distribution in the marine surface sediments of the mudbelt along the west coast of South Africa. Quaternary International 404, 44-56, https://doi.org/10.1016/j.quaint.2015.09.032.

Zhao, X., Dupont, L., Schefuß, E., Meadows, M.E., Hahn, A., Wefer, G., 2016b. Holocene vegetation and climate variability in the winter and summer rainfall zones of South Africa. The Holocene 26, 843-857, https://doi.org/10.1177/0959683615622544.